3-1-1997

Charge and spin dynamics in the one-dimensional t-J_z and t-J models

Shu Zhang
University of Rhode Island

Michael Karbach
University of Rhode Island

Gerhard Müller
University of Rhode Island, gmuller@uri.edu

Joachim Stolze

Citation/Publisher Attribution
Shu Zhang, Michael Karbach, Gerhard Müller, and Joachim Stolze. *Charge and spin dynamics in the one-dimensional t-J_z and t-J models.* Phys. Rev. B **55** (1997), 6491-6503.
Available at: http://dx.doi.org/10.1103/PhysRevB.55.6491

Charge and spin dynamics in the one-dimensional t-J_z and t-J models

Charge and spin dynamics in the one-dimensional t-J_z and t-J models

Shu Zhang,* Michael Karbach, and Gerhard Müller
Department of Physics, The University of Rhode Island, Kingston, Rhode Island 02881-0817

Joachim Stolze
Institut für Physik, Universität Dortmund, 44221 Dortmund, Germany
(Received 11 September 1996)

The impact of the spin-flip terms on the (static and dynamic) charge and spin correlations in the Luttinger-liquid ground state of the one-dimensional (1D) t-J model is assessed by comparison with the same quantities in the 1D t-J_z model, where spin-flip terms are absent. We employ the recursion method combined with a weak-coupling or a strong-coupling continued-fraction analysis. At $J_z/t=0^+$ we use the Pfaffian representation of dynamic spin correlations. The changing nature of the dynamically relevant charge and spin excitations on approach of the transition to phase separation is investigated in detail. At the transition point, the t-J_z ground state has zero (static) charge correlations and very short-ranged (static) spin correlations, whereas the t-J ground state is critical. The t-J_z charge excitations (but not the spin excitations) at the transition have a single-mode nature, whereas charge and spin excitations have a complicated structure in the t-J model. A major transformation of the t-J spin excitations takes place between two distinct regimes within the Luttinger-liquid phase, while the t-J_z spin excitations are found to change much more gradually. In the t-J_z model, phase separation is accompanied by Néel long-range order, caused by the condensation of electron clusters with an already existing alternating up-down spin configuration (topological long-range order). In the t-J model, by contrast, the spin-flip processes in the exchange coupling are responsible for continued strong spin fluctuations (dominated by two-spinon excitations) in the phase-separated state. [S0163-1829(97)06210-3]

I. INTRODUCTION

At the heart of many phenomena in condensed-matter physics is the interplay between the charge and spin degrees of freedom of interacting electrons. The impact of the magnetic ordering and fluctuations on the charge correlations or the effect of the phase separation on the spin correlations, for example, are important issues in the study of strongly correlated electron systems. One of the simplest scenarios in which these questions can be formulated transparently and investigated systematically comprises two successive approximations of the Hubbard model with very strong on-site repulsion. They are known under the names t-J and t-J_z models.[1]

Here we consider a one-dimensional (1D) lattice.[2–9] In both models the assumption is that the Hubbard on-site repulsion is so strong that double occupancy of electrons on any site of the lattice may as well be prohibited completely. This constraint is formally incorporated into the two models by dressing the fermion operators of the standard hopping term with projection operators:

$$H_t=-t\sum_{\sigma=\uparrow,\downarrow}\sum_l \{\tilde{c}^\dagger_{l,\sigma}\tilde{c}_{l+1,\sigma}+\tilde{c}^\dagger_{l+1,\sigma}\tilde{c}_{l,\sigma}\} \tag{1.1}$$

with $\tilde{c}_{l,\sigma}=c_{l,\sigma}(1-n_{l,-\sigma})$, $n_l=n_{l,\uparrow}+n_{l,\downarrow}$, $n_{l,\sigma}=c^\dagger_{l,\sigma}c_{l,\sigma}$. In the t-J model the Hubbard interaction is further taken into account by an isotropic antiferromagnetic exchange coupling between electrons on nearest-neighbor sites:

$$H_{t\text{-}J}=H_t+J\sum_l \{\mathbf{S}_l\cdot\mathbf{S}_{l+1}-\tfrac{1}{4}n_l n_{l+1}\} \tag{1.2}$$

with $S^z_l=\frac{1}{2}(n_{l,\uparrow}-n_{l,\downarrow})$, $S^+_l=\tilde{c}^\dagger_{l,\uparrow}\tilde{c}_{l,\downarrow}$, and $S^-_l=\tilde{c}^\dagger_{l,\downarrow}\tilde{c}_{l,\uparrow}$. In the t-J_z model the isotropic exchange interaction is replaced by an Ising interaction:

$$H_{t\text{-}J_z}=H_t+J_z\sum_l \{S^z_l S^z_{l+1}-\tfrac{1}{4}n_l n_{l+1}\}. \tag{1.3}$$

The absence of spin-flip terms in $H_{t\text{-}J_z}$ introduces additional invariants (not present in $H_{t\text{-}J}$) for the spin configurations of eigenstates and thus alters the relationship between charge and spin correlations considerably. All results presented here will be for one-quarter-filled bands ($N_e=N/2$ electrons on a lattice of N sites).

For weak exchange interaction, both models have a Luttinger-liquid ground state. For stronger interaction, electron-hole phase separation sets in. Phase separation is primarily a transition of the charge degrees of freedom. Here it is driven by an interaction of the spin degrees of freedom, and it is accompanied by a magnetic transition. The degree of spin ordering in the phase-separated state depends on the presence (t-J) or absence (t-J_z) of spin-flip terms in the interaction.

Detailed information on the charge and spin fluctuations in $H_{t\text{-}J}$ and $H_{t\text{-}J_z}$ is contained in the dynamic charge structure factor $S_{nn}(q,\omega)$ and in the dynamic spin structure factor $S_{zz}(q,\omega)$, i.e., in the quantity

$$S_{AA}(q,\omega)\equiv\int_{-\infty}^{+\infty}dt e^{i\omega t}\langle A_q(t)A_{-q}\rangle, \tag{1.4}$$

where A_q stands for the fluctuation operators

$$n_q = N^{-1/2}\sum_l e^{-iql} n_l, \quad S^z_q = N^{-1/2}\sum_l e^{-iql} S^z_l. \quad (1.5)$$

The degree of spin and charge ordering in the ground state is also reflected in the equal-time charge correlation function $\langle n_l n_{l+m}\rangle$ and spin correlation function $\langle S^z_l S^z_{l+m}\rangle$ and in their Fourier transforms, the structure factors $S_{nn}(q)\equiv\langle n_q n_{-q}\rangle$ and $S_{zz}(q)\equiv\langle S^z_q S^z_{-q}\rangle$.

In the following we investigate the $T=0$ charge and spin fluctuations of the two models $H_{t\text{-}J}$ and $H_{t\text{-}J_z}$ in three different regimes with the calculational tools adapted to the situation: the limit of zero exchange coupling (Sec. II), the Luttinger-liquid state (Sec. III), and the phase-separated state (Sec. IV).

II. FREE LATTICE FERMIONS

A. Charge correlations and dynamics

The tight-binding Hamiltonian (1.1) has a highly spin-degenerate ground state. The charge correlations are independent of the spin configurations and, therefore, equivalent to those of a system of spinless lattice fermions,

$$H'_t = -t\sum_l \{c^\dagger_l c_{l+1} + c^\dagger_{l+1} c_l\}. \quad (2.1)$$

This Hamiltonian has been well studied in the context of the 1D $s=1/2$ XX model,

$$H_{XX} = -J_\perp \sum_l \{S^x_l S^x_{l+1} + S^y_l S^y_{l+1}\}, \quad (2.2)$$

which, for $J_\perp = 2t$, becomes Eq. (2.1) via Jordan-Wigner transformation.[10,11] The equal-time charge correlation function of H_t (or H'_t) exhibits power-law decay,

$$\langle n_l n_{l+m}\rangle - \langle n_l\rangle\langle n_{l+m}\rangle = \frac{\cos(\pi m)-1}{2\pi^2 m^2}, \quad (2.3)$$

and the charge structure factor has the form

$$S_{nn}(q) - \frac{N}{4}\delta_{q,0} = \frac{|q|}{2\pi}. \quad (2.4)$$

The dynamic charge structure factor, which is equivalent to the zz dynamic spin structure factor of Eq. (2.2) reads (for $N\to\infty$):[12]

$$S_{nn}(q,\omega) \pi^2\delta(q)\delta(\omega) + \frac{2\Theta(\omega - 2t\,\sin q)\Theta(4t\,\sin(q/2)-\omega)}{\sqrt{16t^2\sin^2(q/2)-\omega^2}}. \quad (2.5)$$

B. Spin correlations

The charge-spin decoupling as is manifest in the product nature of the ground-state wave functions of $H_{t\text{-}J_z}$ at $J_z/t = 0^+$ and $H_{t\text{-}J}$ at $J/t = 0^+$ was shown to lead to a factorization in the spin correlation function.[4,13,14] We can write

$$\langle S^z_l S^z_{l+m}\rangle = \sum_{j=2}^{m+1} C(j-1)P(m,j), \quad (2.6)$$

where $C(m)\equiv\langle S^z_l S^z_{l+m}\rangle_{\rm LS}$ is the correlation function in the ground state of a system of N_e localized spins with antiferromagnetic Heisenberg (t-J) or Ising (t-J_z) coupling, and

$$P(m,j)\equiv\langle n_l n_{l+m}\delta_{j,N_m}\rangle, \quad N_m \equiv \sum_{i=l}^{l+m} n_i$$

is the probability of finding j electrons on sites $l, l+1, \ldots, l+m$ with no holes at the end points of the interval. This expression can be brought into the form

$$\langle S^z_l S^z_{l+m}\rangle = \frac{-1}{4N_e}\sum_{k\neq 0}\frac{S(k)}{\sin^2(k/2)} \times [D_m(k) - 2D_{m-1}(k) + D_{m-2}(k)], \quad (2.7)$$

$$S(k) = \sum_{j=1}^{N_e} e^{ikj} C(j), \quad D_m(k) = \left\langle \exp\left(-ik\sum_{l=0}^{m} n_l\right)\right\rangle, \quad (2.8)$$

where $S(k)$ for $k = (2\pi/N_e)n$, $n = 0, \ldots, N_e - 1$ is the static structure factor for the localized spins, and the $D_m(k)$ are many-fermion expectation values, which are expressible as determinants of dimension $m+1$:[4]

$$D_m(k) = \left| \delta_{ij} - \frac{(1+e^{-ik})}{2N_e}\frac{\sin[\pi(i-j)/2]}{\sin[\pi(i-j)/2N_e]}\right|_{i,j=0,\ldots,m}.$$

In $H_{t\text{-}J_z}$ we have $C(m) = (1/4)(-1)^m$, i.e., $S(k) = (N_e/4)\delta_{k,\pi}$, reflecting the (invariant) alternating up-down sequence of successive electron spins. Expression (2.7) can then be evaluated in closed form:

$$\langle S^z_l S^z_{l+2n}\rangle = \frac{(-1)^n}{2\pi^2}\prod_{i=1}^{n-1} P_i^2, \quad (2.9a)$$

$$\langle S^z_l S^z_{l+2n+1}\rangle = -\tfrac{1}{2}(\langle S^z_l S^z_{l+2n}\rangle + \langle S^z_l S^z_{l+2n+2}\rangle) \quad (2.9b)$$

with

$$P_i = \frac{2}{\pi}\prod_{j=1}^{i}\left(1 - \frac{1}{4j^2}\right)^{-1}.$$

The leading terms of the long-distance asymptotic expansion of (2.9) are[15]

$$\langle S^z_l S^z_{l+m}\rangle_{t\text{-}J_z} \xrightarrow{m\to\infty} \frac{A^2}{4\sqrt{2}}\frac{1}{\sqrt{|m|}} \times\left[\left(1 - \frac{1}{8}\frac{1}{m^2}\right)\cos\frac{m\pi}{2} - \frac{1}{2m}\sin\frac{m\pi}{2}\right] \quad (2.10)$$

with $A = 2^{1/12}\exp[3\zeta'(-1)] = 0.64500\ldots$. The structure of $D_m(\pi)$ is very similar to that of the xx spin-correlation function of H_{XX}.[10,16,17] Its leading asymptotic term has the form $\langle S^x_l S^x_{l+m}\rangle_{XX} \sim (A^2/2\sqrt{2})m^{-1/2}$.

In $H_{t\text{-}J}$ the spin-flip terms weaken the spin correlations at $J/t = 0^+$. The function $S(k)$ in Eq. (2.7) is determined via

Eq. (2.8) by the spin correlation function of the 1D $s=1/2$ Heisenberg antiferromagnet (XXX model). Its leading asymptotic term reads[18] $C(m)\sim\Gamma(-1)^m m^{-1}(\ln m)^{1/2}$ with amplitude $\Gamma\simeq 0.125(15)$ as estimated from finite-chain data.[19] The leading asymptotic term of the t-J spin correlation function inferred from Eq. (2.7) has the form[13]

$$\langle S_l^z S_{l+m}^z\rangle_{t\text{-}J}\sim\Gamma A^2\sqrt{2}\cos(\pi m/2)\frac{(\ln m)^{1/2}}{m^{3/2}}. \quad (2.11)$$

The t-J and t-J_z spin structure factors $S_{zz}(q)$ inferred from the results presented here will be presented and discussed in Sec. III E.

For an intuitive understanding of the $q=\pi$ charge density wave in the ground state at $J_z/t=0^+$ and $J/t=0^+$, we note that the hopping term opposes electron clustering. In the absence of the exchange term, which favors clustering of electrons with opposite spin, the hopping effectively causes an electron repulsion. This is reflected in the power-law decay (2.3) of the charge correlation function, specifically in the term which oscillates with a period equal to twice the lattice constant ($q=4k_F=\pi$). In this state, an electron is more likely to have a hole next to it than another electron.

How does this affect the spin correlations? Recall that the ground state of $H_{t\text{-}J_z}$ at $J_z/t=0^+$ is characterized by an (invariant) alternating spin sequence. In a perfect electron cluster this sequence would amount to saturated Néel ordering ($q=\pi$), but here it is destroyed by a distribution of holes. Spin long-range order exists only in a topological sense. However, some amount of actual spin ordering survives by virtue of the effective electron repulsion in the form of the algebraically decaying term (2.10) in the spin correlation function with a wavelength equal to four times the lattice constant ($q=2k_F=\pi/2$).

A similar argument obtains for the t-J model. Since its ground state at $J/t=0^+$ contains all spin sequences with $S_T^z=0$, not just the alternating ones, the resulting $q=\pi/2$ oscillations (2.11) in the spin correlation function decay more rapidly than in the t-J_z case.[20]

C. Spin dynamics

Expression (2.6) cannot be generalized straightforwardly for the calculation of *dynamic* spin correlations, the principal reason being that the number of electrons between any two lattice sites is not invariant under time evolution. However, in the t-J_z case we can determine the function $\langle S_l^z(t)S_{l+m}^z\rangle$ on a slight detour. We use open boundary conditions and write

$$S_l^z=-\frac{1}{2}\sigma_L\prod_{i=1}^{l}(-1)^{n_i}n_l, \quad (2.12)$$

where $\sigma_L=\pm 1$ denotes the spin direction of the leftmost particle in the chain, which *is* an invariant under time evolution. The time-dependent two-spin correlation function of the open-ended t-J_z chain is then related to the following many-fermion correlation function:

$$\langle S_l^z(t)S_{l+m}^z\rangle=\frac{1}{4}\left\langle n_l(t)\prod_{i=1}^{l}(-1)^{n_i(t)}\prod_{j=1}^{l+m}(-1)^{n_j}n_{l+m}\right\rangle$$
$$=\langle c_l^\dagger(t)c_l(t)A_1(t)B_1(t)A_2(t)B_2(t)\cdots A_l(t)B_l(t)A_1B_1A_2B_2\cdots A_{l+m}B_{l+m}c_{l+m}^\dagger c_{l+m}\rangle$$

with $A_l\equiv c_l^\dagger+c_l$, $B_l\equiv c_l^\dagger-c_l$. In order to extract the bulk behavior of $\langle S_l^z(t)S_{l+m}^z\rangle$ from this expression, we must choose both sites l and $l+m$ sufficiently far from the boundaries.

The numerical evaluation of this function via Pfaffians shows[21–23] that the leading long-time asymptotic term describes uniform power-law decay, $\langle S_l^z(t)S_{l+2n}^z\rangle\sim t^{-1/2}$, for even distances and (more rapid) oscillatory power-law decay, $\langle S_l^z(t)S_{l+2n+1}^z\rangle\sim e^{-2it}t^{-\alpha}$, $\alpha\gtrsim 1$, for odd distances. Moreover, we have found compelling numerical evidence that the relation (2.9b) can be generalized to time-dependent correlation functions in the bulk limit $l\to\infty$.

Our data for the dynamic correlations in conjunction with the long-distance asymptotic result (2.10) for the static correlations suggest that the leading term for large distances and long times has the form[24]

$$\langle S_l^z(t)S_{l+m}^z\rangle_{t\text{-}J_z}\sim\frac{1}{4}\frac{A^2/\sqrt{2}}{(m^2-4t^2)^{1/4}}\cos\frac{\pi m}{2}, \quad (2.13)$$

which is, apart from the spatial oscillations, similar to the corresponding (exact) asymptotic result in the XX model:[17,25]

$$\langle S_l^x(t)S_{l+m}^x\rangle_{XX}\sim\frac{1}{4}\frac{A^2\sqrt{2}}{(m^2-J_\perp^2t^2)^{1/4}}. \quad (2.14)$$

The asymptotic behavior (2.13) of the dynamic spin correlation function implies that the dynamic spin structure factor has a divergent infrared singularity at $q=\pi/2$: $S_{zz}(\pi/2,\omega)_{t\text{-}J_z}\sim\omega^{-1/2}$. Further evidence for this singularity and for a corresponding singularity in $S_{zz}(q,\omega)_{t\text{-}J}$ will be presented in Sec. III F.

III. LUTTINGER-LIQUID STATE

Turning on the exchange interaction in $H_{t\text{-}J}$ and $H_{t\text{-}J_z}$, which is attractive for electrons with unlike spins and zero otherwise, alters the charge and spin correlations in the ground state gradually over the range of stability of the Luttinger-liquid state. In the t-J_z model, where successive electrons on the lattice have opposite spins, the exchange coupling counteracts the effectively repulsive force of the hopping term and thus gradually weakens the enhanced $q=\pi$ charge and $q=\pi/2$ spin correlations. We shall see that

the repulsive and attractive forces reach a perfect balance at $J_z/t=4^-$. Here the distribution of electrons (or holes) is completely random. All charge pair correlations vanish identically and all spin pair correlations too, except those between nearest-neighbor sites. This state marks the boundary of the Luttinger-liquid phase. At $J_z/t>4$ the attractive nature of the resulting force between electrons produces new but different charge and spin correlations in the form of charge long-range order at $q=0^+$ (phase separation) and spin long-range order at $q=\pi$ (antiferromagnetism).

In the t-J model the disordering and reordering tendencies are similar, but the exchange interaction with spin-flip processes included is no longer uniformly attractive. At no point in parameter space do the attractive and repulsive forces cancel each other and produce a random distribution of electrons. A sort of balance between these forces exists at $J/t=2$, which is reflected in the observation[9] that the ground state is particularly well represented by a Gutzwiller wave function at this coupling strength. Charge and spin correlations exhibit power-law decay at the endpoint, $J/t\simeq 3.2$, of the Luttinger-liquid phase. Here the attractive forces start to prevail on account of sufficiently strong antiferromagnetic short-range correlations and lead to phase separation, but the spin correlations continue to decay to zero asymptotically at large distances.

One characteristic signature of a Luttinger liquid is the occurrence of infrared singularities with interaction-dependent exponents in dynamic structure factors. In the following we present direct evidence for interaction-dependent infrared singularities in the dynamic charge and spin structure factors of $H_{t\text{-}J_z}$ and $H_{t\text{-}J}$. We employ the recursion method[26] in combination with techniques of continued-fraction analysis recently developed in the context of magnetic insulators.[27–30]

The recursion algorithm in the present context is based on an orthogonal expansion of the wave function $|\Psi_q^A(t)\rangle \equiv A_q(-t)|\phi\rangle$ with A_q as defined in Eq. (1.5). It produces (after some intermediate steps) a sequence of continued-fraction coefficients $\Delta_1^A(q),\Delta_2^A(q),\ldots$ for the relaxation function,

$$c_0^{AA}(q,z)=\cfrac{1}{z+\cfrac{\Delta_1^A(q)}{z+\cfrac{\Delta_2^A(q)}{z+\ldots}}}, \tag{3.1}$$

which is the Laplace transform of the symmetrized correlation function $\Re\langle A_q(t)A_{-q}\rangle/\langle A_qA_{-q}\rangle$. The $T=0$ dynamic structure factor (1.4) is then obtained via

$$S_{AA}(q,\omega)=4\langle A_qA_{-q}\rangle\Theta(\omega)\lim_{\varepsilon\to 0}\Re[c_0^{AA}(q,\varepsilon-i\omega)].$$

For some aspects of this study, we benefit from the close relationship of the two itinerant electron models $H_{t\text{-}J_z}$ and $H_{t\text{-}J}$ with the 1D $s=1/2$ XXZ model,

$$H_{XXZ}=H_{XX}-J_\parallel\sum_l S_l^zS_{l+1}^z,$$

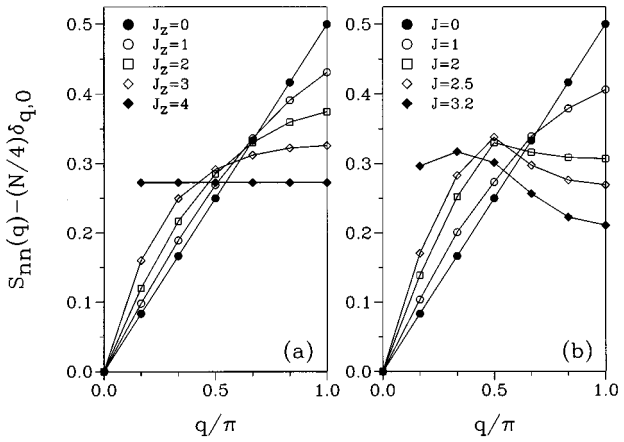

FIG. 1. Static charge structure factor at $T=0$ of (a) the t-J_z model and (b) t-J model in the Luttinger-liquid phase. Results extracted from the ground-state wave function determined numerically for a system of $N=12$ sites.

a model for localized electron spins. The equivalence of $H_{t\text{-}J_z}$ and H_{XXZ} for $J_\parallel=J_z/2$ and $J_\perp=2t$ was pointed out and used before.[7,4] Depending on the boundary conditions, it can be formulated as a homomorphism between eigenstates belonging to specific invariant subspaces of the two models. The mapping assigns to any up spin and down spin in H_{XXZ} an electron and a hole, respectively, in $H_{t\text{-}J_z}$. The spin sequence of the electrons in the subspace of interest here is fixed, namely alternatingly up and down. The importance of this mapping derives from the fact that the ground-state properties of H_{XXZ} have been analyzed in great detail.[31–33]

The $T=0$ dynamic charge structure factor $S_{nn}(q,\omega)$ of $H_{t\text{-}J_z}$ is thus equivalent to the $T=0$ dynamic spin structure factor $S_{zz}(q,\omega)$ of H_{XXZ} throughout the Luttinger-liquid phase, and we shall take advantage of the results from previous studies of XXZ spin dynamics.[34,35] The spin dynamics of $H_{t\text{-}J_z}$ is not related to any known dynamical properties of H_{XXZ}.

A. Charge structure factor

Certain dominant features of the dynamic charge structure factor $S_{nn}(q,\omega)$ are related to known properties of the static charge structure factor. Figure 1 displays finite-N data of $S_{nn}(q)$ for various coupling strengths in the Luttinger-liquid phase of (a) $H_{t\text{-}J_z}$ and (b) $H_{t\text{-}J}$.

The alignment of the data points on a sloped straight line in the free-electron limit represents the exact result (2.4), which is common to both models. The persistent linear behavior at small q for nonzero coupling reflects an asymptotic term of the form $\sim A_0m^{-2}$ in the charge correlation function $\langle n_ln_{l+m}\rangle$, while the progressive weakening of the cusp singularity at $q=\pi$ reflects an asymptotic term of the form $\sim A_1\cos(\pi m)/m^{\eta_\rho}$ with a coupling-dependent charge correlation exponent η_ρ. For $H_{t\text{-}J_z}$ this exponent is exactly known:[33]

$$\eta_\rho=2/[1-(2/\pi)\arcsin(J_z/4t)]. \tag{3.2}$$

No exact result exists for the t-J case, but the prediction is that the charge correlation exponent varies over the same range of values,[5] i.e., between $\eta_\rho=2$ at $J/t=0$ and $\eta_\rho=\infty$ at $J/t\simeq 3.2$. For $J/t\gtrsim 1$, the data in Fig. 1(b) indicate the presence of a third cusp singularity in $S_{nn}(q)$, namely at $q=\pi/2$, which reflects the third asymptotic term, $\sim A_2\cos(\pi m/2)/m^{1+\eta_\rho/4}$, predicted for the t-J charge correlations.[36] No corresponding singularity is indicated in the data of Fig. 1(a), nor is any corresponding asymptotic term predicted in the XXZ spin correlations.

At the endpoint of the Luttinger-liquid phase ($J_z/t=4$), the t-J_z ground-state wave function has the form

$$|\phi_0\rangle=\sum_{1\le l_1<l_2<\ldots<l_{N/2}\le N}\binom{N}{N/2}^{-1/2}|l_1,\ldots,l_{N/2}\rangle \times\frac{1}{\sqrt{2}}\{|\uparrow\downarrow\uparrow\ldots\rangle-|\downarrow\uparrow\downarrow\ldots\rangle\}, \tag{3.3}$$

where $|l_1,\ldots,l_{N/2}\rangle$ specifies the variable charge positions. It corresponds to the vector with total spin $S_T=N/2$ and z component $S_T^z=0$ of the degenerate XXZ ground state at $J_\parallel/J_\perp=1$. The electrons are distributed completely at random on the lattice, while the sequence of spin orientations is frozen in a perfect up-down pattern. This state is nondegenerate for finite N, and its energy per site is N independent: $E_0/N=-t$. For $N\to\infty$, the t-J_z charge correlations disappear completely, $\langle n_l n_{l+m}\rangle-\langle n_l\rangle\langle n_{l+m}\rangle=\delta_{m,0}/4$ as is indicated by the finite-N data for $J_z/t=4$ in Fig. 1(a): $S_{nn}(q)-(N/4)\delta_{q,0}=[N/4(N-1)](1-\delta_{q,0})$. The t-J charge correlations, by contrast, seem to persist at $J/t\simeq 3.2$.

B. Charge dynamics (weak-coupling regime)

Expression (2.5) for the $T=0$ dynamic charge structure factor $S_{nn}(q,\omega)$ of H_t is modified differently under the influence of a J_z-type or a J-type exchange interaction. Within the Luttinger-liquid phase we distinguish two regimes for the charge dynamics: a *weak-coupling* regime and a *strong-coupling* regime. In the weak-coupling regime, the interaction produces only small and gradual changes in $S_{nn}(q,\omega)$, which are accessible to perturbation calculations. That is no longer the case in the strong-coupling regime, where changes of a more qualitative nature are likely to take place. In the context of the recursion method, the two regimes can be diagnosed by a technical criterion, namely the growth of the sequence of continued-fraction coefficients $\Delta_k^A(q)$ in Eq. (3.1).[29]

In the framework of a weak-coupling continued-fraction (WCCF) analysis, the dynamically dominant excitation spectrum of $S_{nn}(q,\omega)$ is confined to a continuum as in Eq. (2.5) but with modified boundaries and a rearranged spectral-weight distribution. Moreover, a discrete branch of excitations appears outside the continuum. A WCCF analysis for $S_{nn}(\pi,\omega)$ of $H_{t\text{-}J}$ and, in disguise, also of $H_{t\text{-}J_z}$, namely in the form of $S_{zz}(\pi,\omega)$ for H_{XXZ} was reported in Ref. 29, mainly for the purpose of calculating line shapes.

The renormalized bandwidth ω_0 of the dynamic charge structure factor $S_{nn}(\pi,\omega)$ versus the coupling constant as obtained from a WCCF analysis is shown in the main plot of Fig. 2 for both the t-J_z model (□) and the t-J model (○). In the XXZ context, ω_0 is the bandwidth of the two-spinon continuum, which is exactly known.[32] Translated into t-J_z terms, the expression reads

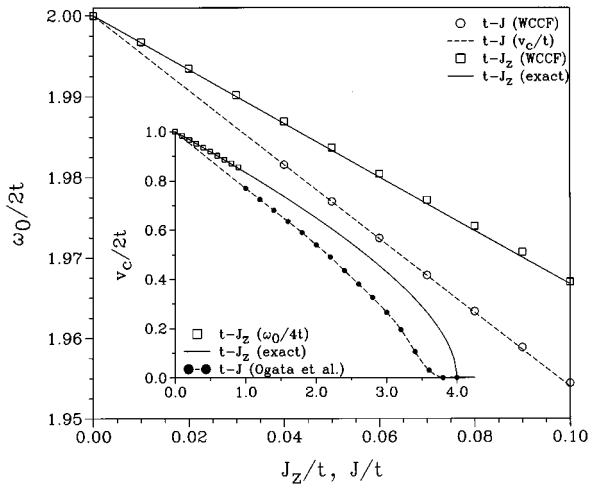

FIG. 2. Main plot: Renormalized bandwidth of the dynamically relevant charge excitations in the weak-coupling regime of the Luttinger-liquid phase of the t-J and t-J_z models. Inset: Charge velocity in the two models over the full range of the Luttinger-liquid phase. The open symbols represent weak-coupling continued-fraction data and the solid lines represent the exact expression (3.4). The full circles are finite-chain data from Ref. 5.

$$\omega_0/2t=(\pi/\mu)\sin\mu,\quad \cos\mu=-J_z/4t \tag{3.4}$$

and is represented by the solid line. Comparison with our data confirms the reliability of the WCCF analysis.

Our bandwidth data for the t-J model can be compared with numerical results of Ogata *et al.*[5] for the charge velocity v_c as derived from the numerical analysis of finite chains. The underlying assumption is that the relation $\omega_0=2v_c$, which is exact in $H_{t\text{-}J_z}$, also holds for $H_{t\text{-}J}$. The t-J charge-velocity results of Ref. 5 over the entire range of the Luttinger-liquid phase are shown as full circles connected by a dashed line in the inset. The solid line represents the exact t-J_z charge velocity $v_c=\omega_0/2$ with ω_0 from Eq. (3.4).

The dashed line in the main plot is the t-J bandwidth prediction inferred from the data of Ref. 5. It is in near perfect agreement with the WCCF data (○). The open squares in the inset show the WCCF data over a wider range of coupling strengths. The renormalized bandwidth ω_0 will shrink to zero at the endpoint of the Luttinger-liquid phase, and the spectral weight will gradually be transferred from the shrinking continuum to states of a different nature at higher energies.

C. Infrared exponent

In the Luttinger-liquid phase, the dynamic charge structure factor has an infrared singularity with an exponent related to the charge correlation exponent:

$$S_{nn}(\pi,\omega)\sim\omega^{\beta_\rho},\quad \beta_\rho=\eta_\rho-2\,. \tag{3.5}$$

The WCCF analysis yields specific predictions for β_ρ in both models. Our results plotted versus coupling constant are

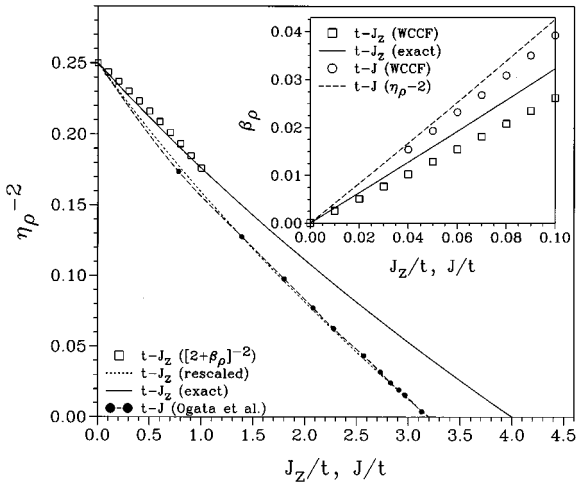

FIG. 3. Inset: Infrared exponent β_ρ as defined by Eq. (3.5) in the weak-coupling regime of the Luttinger-liquid phase of the t-J and t-J_z models. Main plot: Inverse square of the charge correlation exponent for both models over the full range of the Luttinger-liquid phase. The open symbols represent weak-coupling continued-fraction data, the solid lines represent the exact expression (3.2), and the short-dashed line the same expression with $J/3.2t$ substituted for $J_z/4t$. The full circles are the finite-chain data from Ref. 5.

shown in the inset to Fig. 3 for $H_{t\text{-}J_z}$ (□) and $H_{t\text{-}J}$ (○). The solid line represents the exact t-J_z result inferred from Eq. (3.2).

We observe that the WCCF prediction for the infrared exponent (□) rises somewhat more slowly from zero with increasing coupling than the exact result. The solid line in the main plot depicts the inverse square of the exact t-J_z correlation exponent (3.2) over the entire range of the Luttinger-liquid phase. The open squares represent the WCCF data for $2+\beta_\rho=\eta_\rho$ extended to stronger coupling. For $H_{t\text{-}J}$ the correlation exponent is not exactly known. The solid circles interpolated by the dashed line represent the prediction for η_ρ of Ogata *et al.*[5] based on a finite-size analysis. The dashed line in the inset is inferred from the same data. It agrees reasonably well with the WCCF data for β_ρ (○).

The solid and long-dashed curves in the main plot suggest the intriguing possibility that the exponents η_ρ of the two models have the same dependence on the scaled coupling constants $J_z/J_z^{(c)}$ with $J_z^{(c)}=4t$ and $J/J^{(c)}$ with $J^{(c)}\simeq 3.2t$. The short-dashed line represents the exact t-J_z result (3.2) thus transcribed for $H_{t\text{-}J}$. Its deviation from the data of Ogata *et al.* is very small throughout the Luttinger-liquid phase.

In Ref. 29 we carried out a WCCF reconstruction of the function $S_{nn}(\pi,\omega)$ for the t-J model and the t-J_z model (alias XXZ model).[37] The observed spectral-weight distributions of both models consisted of a gapless continuum with a cusplike infrared singularity ($\beta_\rho>0$), a shrinking bandwidth ($\omega_0/2t<2$), and a lone discrete state outside the continuum near its upper boundary.

D. Charge dynamics (strong-coupling regime)

What happens to the dynamic charge structure factor $S_{nn}(q,\omega)$ as the exchange interaction is increased beyond the weak-coupling regime of the Luttinger-liquid phase? For the t-J_z case the answer can be inferred from known results for the spin dynamics of H_{XXZ}.[34,35] The continuum of charge excitations with sine-like boundaries

$$\epsilon_L(q)=\frac{\pi t\,\sin\mu}{\mu}|\sin q|,\quad \epsilon_U(q)=2\epsilon_L(q/2),$$

continues to shrink to lower and lower energies, and discrete branches of excitations

$$\epsilon_n(q)=\frac{2\pi t\,\sin\mu}{\mu\,\sin y_n}\sin\frac{q}{2}\sqrt{\sin^2\frac{q}{2}+\sin^2 y_n\cos^2\frac{q}{2}}$$

with $y_n=(\pi n/2\mu)(\pi-\mu)$ emerge successively at $\mu=\pi/(1+1/n)$ from the upper continuum boundary.[38,35] All these excitations carry some spectral weight, at least for finite N, but most of the spectral weight in $S_{nn}(q,\omega)$ is transferred from the shrinking continuum to the top branch, the one already present in the WCCF reconstruction.[29]

At the endpoint of the Luttinger-liquid phase $J_z/t=4$, the continuum states have been replaced by a series of branches $\epsilon_n(q)=(2t/n)(1-\cos q)$, $n=1,2,\ldots$, all the spectral weight is carried by the top branch ($n=1$), and the dynamic charge structure factor reduces to the single-mode form

$$S_{nn}(q,\omega)=\pi^2\delta(q)\,\delta(\omega)+\frac{\pi}{2}\,\delta\left(\omega-J_z\sin^2\frac{q}{2}\right).$$

In the framework of the recursion method applied to the exact finite-size ground state (3.3), this simple result follows from a spontaneously terminating continued fraction with coefficients $\Delta_1(q)=J_z^2\sin^4(q/2)$, $\Delta_2(q)=0$.

The dynamically relevant charge excitation spectrum of $H_{t\text{-}J}$, which has an even more complex structure, will be presented in a separate study. In this case, exact results exist only at one point ($J/t=2$) in the strong-coupling regime.[7]

E. Spin structure factor

The long-distance asymptotic behavior of the t-J spin correlation function in the Luttinger-liquid phase was predicted to be governed by two leading power-law terms of the form[2–5]

$$\langle S_l^z S_{l+m}^z\rangle_{t\text{-}J}\sim B_1\frac{1}{m^2}+B_2\frac{\cos(\pi m/2)}{m^{\eta_\rho/4+1}},\qquad (3.6)$$

where η_ρ is the charge correlation exponent discussed previously. The open circles in Fig. 4(a) depict the spin structure factor $S_{zz}(q)_{t\text{-}J}$ for $J/t=0^+$ of a system with $N=56$ sites as inferred via numerical Fourier transform from the results for the spin correlation function presented in Sec. II. The two asymptotic terms of Eq. (3.6) are reflected, respectively, in the linear behavior at small q and in the pointed maximum at $q=\pi/2$. The latter turns into a square-root cusp as $N\to\infty$. The extrapolated maximum is $S_{zz}(\pi/2)_{t\text{-}J}=0.28(1)$ (indicated by a + symbol). The extrapolated slope at $q=0$ is $S_{zz}(q)_{t\text{-}J}/q=0.0847(20)$. The observed smooth minimum at $q=\pi$ suggests that $S_{zz}(q)_{t\text{-}J}$, unlike $S_{nn}(q)_{t\text{-}J}$, has no singularity there. The extrapolated value is $S_{zz}(\pi)_{t\text{-}J}=0.127\,019(2)$.

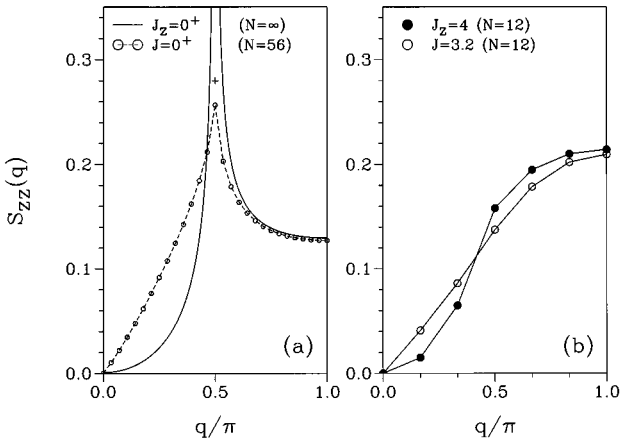

FIG. 4. Static spin structure factor at $T=0$ of the t-J_z and t-J models (a) in the free-electron limit and (b) at the transition to phase separation. The data for $J_z=0^+$ are calculated via numerical Fourier transform of expression (2.9). The data for $J=0^+$ are derived from expression (2.7) as explained in the text. The remaining results are extracted from the ground-state wave function determined numerically for systems of $N=12$ sites.

The predictions of Eq. (3.6) that the linear behavior in $S_{zz}(q)_{t\text{-}J}$ at small q persists throughout the Luttinger-liquid phase and that the cusp singularity at $q=\pi/2$ weakens with increasing J/t and disappears at the onset of phase separation are consistent with our result for $J/t=3.2$, plotted in Fig. 4(b). The open circles suggest a smooth curve which rises linearly from zero at $q=0$. The smooth extremum at $q=\pi$ has turned from a minimum at $J/t=0^+$ into a maximum at $J/t=3.2$.

The solid line in Fig. 4(a) represents $S_{zz}(q)_{t\text{-}J_z}$ for the free-fermion case $J_z/t=0^+$ as obtained from Fourier transforming Eq. (2.9). It differs from the corresponding t-J result (○) mainly in three aspects: (i) the rise from zero at small q is quadratic instead of linear, reflecting nonsingular behavior at $q=0$, i.e., the absence of a nonoscillatory power-law asymptotic term in $\langle S^z_l S^z_{l+m}\rangle_{t\text{-}J_z}$; (ii) the singularity at $q=\pi/2$ is divergent: $\sim|q-\pi/2|^{-1/2}$; (iii) the smooth local minimum at $q=\pi$ has a slightly higher value, $S_{zz}(\pi)_{t\text{-}J_z}\simeq 0.129$.

Over the range of the Luttinger-liquid phase, the asymptotic term in $\langle S^z_l S^z_{l+m}\rangle_{t\text{-}J_z}$ which governs the singularity in $S_{zz}(q)_{t\text{-}J_z}$ at $q=\pi/2$ is of the form $\sim B_2\cos(\pi m/2)/m^{\eta_\rho/4}$. As in the t-J case, the singularity weakens gradually and then disappears at the transition point, $J_z/t=4$. The finite-N result of $S_{zz}(q)_{t\text{-}J_z}$ at $J_z/t=4$, (●) in Fig. 4(b), indeed suggests a curve with no singularities. This is confirmed by the exact result,

$$S_{zz}(q)_{t\text{-}J_z}=\tfrac{1}{8}(1-\cos q), \tag{3.7}$$

inferred from the exact ground-state wave function (3.3) for $N\to\infty$. It reflects a spin correlation function which vanishes for all distances beyond nearest neighbors.

F. Spin dynamics

Under mild assumptions, which have been tested for $H_{t\text{-}J_z}$ at $J_z/t=0^+$, the following properties of the dynamic spin structure factors $S_{zz}(q,\omega)$ of $H_{t\text{-}J}$ or $H_{t\text{-}J_z}$ can be inferred from the singularity structure of $S_{zz}(q)$: (i) The excitation spectrum in $S_{zz}(q,\omega)$ is gapless at $q=\pi/2$. (ii) The spectral-weight distribution at the critical wave number $q=\pi/2$ has a singularity of the form:

$$S_{zz}\left(\frac{\pi}{2},\omega\right)_{t\text{-}J_z}\sim\omega^{\eta_\rho/4-2},\quad S_{zz}\left(\frac{\pi}{2},\omega\right)_{t\text{-}J}\sim\omega^{\eta_\rho/4-1}.$$

In the weak-coupling limit ($\eta_\rho=2$), this yields $\sim\omega^{-3/2}$ for $H_{t\text{-}J_z}$ and $\sim\omega^{-1/2}$ for $H_{t\text{-}J}$. In both cases, the infrared exponent increases with increasing coupling. A landmark change in $S_{zz}(\pi,\omega)$ occurs at the point where the infrared exponent switches sign (from negative to positive). In the t-J_z case this happens for $\eta_\rho=8$ and in the t-J case for $\eta_\rho=4$. According to the data displayed in Fig. 3, this corresponds to the coupling strengths $J_z/t=3.6955\ldots$ and $J/t\simeq 2.3$, respectively.

The dynamic spin structure factor $S_{zz}(q,\omega)_{t\text{-}J_z}$ as obtained via the recursion method combined with a strong-coupling continued-fraction (SCCF) analysis[27,28] is plotted in Fig. 5 as a continuous function of ω and a discrete function of $q=2\pi m/N$, $m=0,\ldots,N/2$ with $N=12$ for coupling strengths $J_z/t=0^+,2,3,4$. This function has a nongeneric ($q\leftrightarrow\pi-q$) symmetry, which obtains for the dynamically relevant excitation spectrum and for the line shapes, but not for the integrated intensity.[39] In the weak-coupling limit, $J_z/t=0^+$, the spectral weight in $S_{zz}(q,\omega)$ is dominated by fairly well defined excitations at all wave numbers. The dynamically relevant dispersion is $|\cos q|$-like.

With J_z/t increasing toward the endpoint of the Luttinger-liquid phase, the following changes can be observed in $S_{zz}(q,\omega)$: The peaks at $q\neq\pi/2$ gradually grow in width and move toward lower frequencies. The $|\cos q|$-like dispersion of the peak positions stays largely intact, but the amplitude shrinks steadily. The central peak at the critical wave number $q=\pi/2$ starts out with large intensity and slowly weakens with increasing coupling. Between $J_z/t=3$ and $J_z/t=4$, it turns rather quickly into a broad peak, signaling the expected change in sign of the infrared exponent.

The dynamically relevant dispersion of the dominant spin fluctuations as determined by the peak positions in our SCCF data for $S_{zz}(q,\omega)$ is shown in Fig. 6 for several values of J_z/t. The linear initial rise from zero at $q=\pi/2$ is typical of a Luttinger liquid. The amplitude of the $|\cos q|$-like dispersion decreases with increasing J_z/t and approaches zero at the transition to phase separation. At the same time, the line shapes of $S_{zz}(q,\omega)_{t\text{-}J_z}$ tend to broaden considerably. These trends are not shared with the t-J spin excitations as we shall see.

The SCCF analysis indicates that the Luttinger-liquid phase of the t-J model can be divided into two regimes with distinct spin dynamical properties. For coupling strengths $0<J/t\lesssim 1$, the function $S_{zz}(q,\omega)_{t\text{-}J}$, which is plotted in Fig. 7, exhibits some similarities with the corresponding t-J_z results. The main commonality is a well-defined spin mode at not too small wave numbers with a $|\cos q|$-like dispersion.

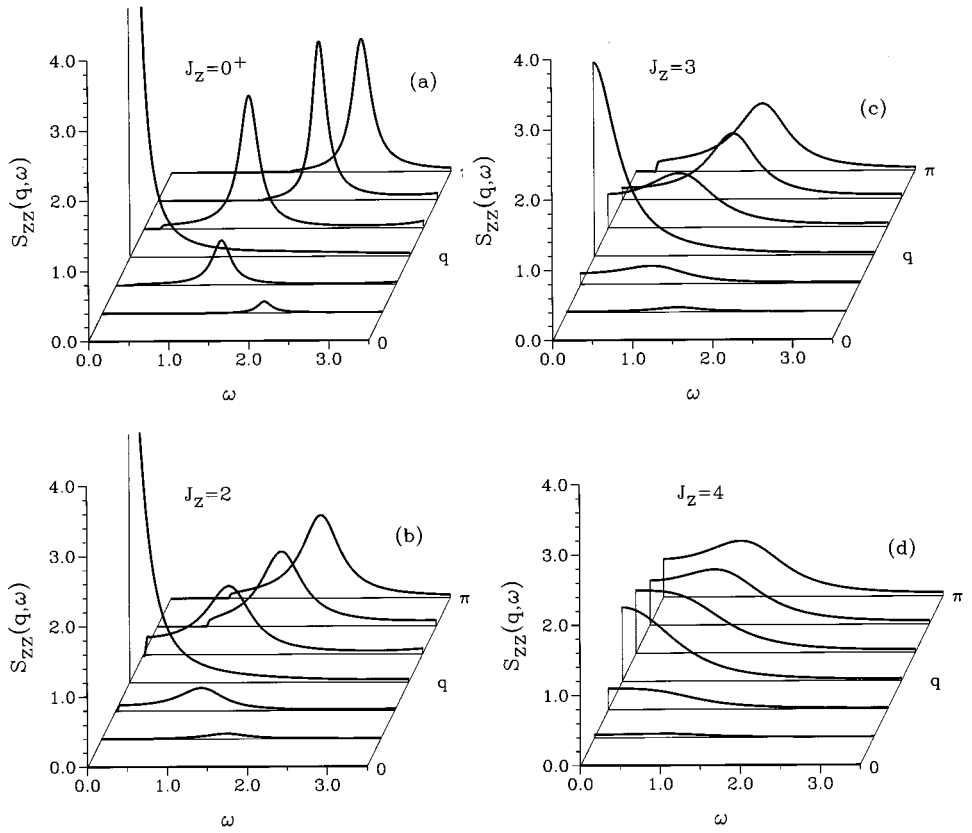

FIG. 5. Dynamic spin structure factor $S_{zz}(q,\omega)$ at $T=0$ in the Luttinger-liquid phase of the t-J_z model. The results for $t=1$ and four different values of J_z are obtained via strong-coupling continued-fraction reconstruction from the coefficients $\Delta_1,\ldots,\Delta_6$ and an unbounded gap terminator (Refs. 27,28). The Δ_k's are extracted from the ground-state wave function for a system of $N=12$ sites.

This dispersion is displayed in the main plot of Fig. 8 for different J/t values within this first regime of the Luttinger-liquid phase.

However, even in the common features, the differences cannot be overlooked: (i) The $(q\leftrightarrow\pi-q)$ symmetry in the line shapes of $S_{zz}(q,\omega)_{t\text{-}J_z}$ is absent in $S_{zz}(q,\omega)_{t\text{-}J}$. (ii) The amplitude of the $|\cos q|$-like dispersion grows with increasing J/t, contrary to the trend observed in Fig. 6 for the corresponding t-J_z spin dispersion. (iii) The gradual upward shift of the peak position in $S_{zz}(\pi,\omega)_{t\text{-}J}$ is accompanied by a significant increase in line width (see inset to Fig. 9). Over the range $0\lesssim J/t\lesssim 1.25$, the trend of the $q=\pi$ spin mode is opposite to what one expects under the influence of an antiferromagnetic exchange interaction of increasing strength. (iv) The intensity of the central peak in $S_{zz}(\pi/2,\omega)_{t\text{-}J}$ is considerably weaker than in in $S_{zz}(\pi/2,\omega)_{t\text{-}J_z}$. The peak turns shallow and disappears quickly with increasing coupling (see Fig. 9, main plot). This observation is in accord with the proposed dependences of the infrared exponents on the coupling constants. (v) The linear dispersion of the dynamically relevant spin excitations have markedly different slopes above and below the critical wave number $q=\pi/2$ (Fig. 8, main plot). At long wavelengths the spectral weight in $S_{zz}(q,\omega)_{t\text{-}J}$ is concentrated at much lower frequencies than in $S_{zz}(q,\omega)_{t\text{-}J_z}$.[40]

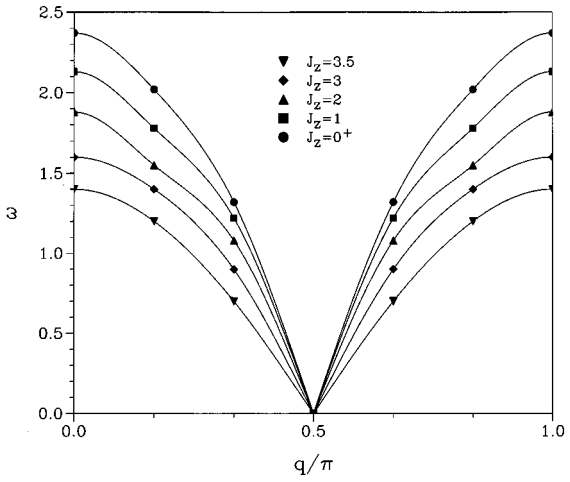

FIG. 6. Dynamically relevant dispersions of the excitations dominating the dynamic spin structure factor $S_{zz}(q,\omega)$ at $T=0$ for $t=1$ and different values of J_z within the Luttinger-liquid phase of the t-J_z model. The symbols, which are smoothly interpolated by solid lines, represent the peak positions of results such as shown in Fig. 5.

As the coupling strength increases past the value $J/t\simeq 0.75$, the spin modes which dominate $S_{zz}(q,\omega)_{t\text{-}J}$ in the first regime of the Luttinger-liquid phase broaden rapidly and lose their distinctiveness. There is a crossover region between the first and second regime, which roughly comprises the coupling range $1\lesssim J/t\lesssim 2$. Over that range, the spin dynamic structure factor tends to be governed by complicated structures with rapidly moving peaks.

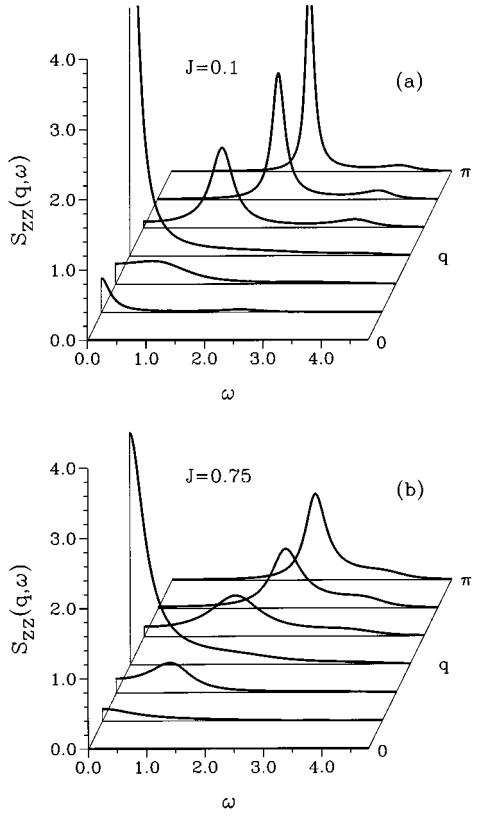

FIG. 7. Dynamic spin structure factor $S_{zz}(q,\omega)$ at $T=0$ for $t=1$ and two values of J in the first regime of the Luttinger-liquid phase of the t-J model. The results are obtained by the same method as those of Fig. 5.

At the end of the crossover region, a new type of spin mode with an entirely different kind of dispersion has gained prominence in $S_{zz}(q,\omega)_{t\text{-}J}$, and it stays dominant throughout the remainder of the Luttinger-liquid phase. This is illustrated in Fig. 10 for three J/t values in the second regime of the Luttinger-liquid phase. The dispersion of these new spin modes gradually evolves with increasing coupling strength as shown in the inset to Fig. 8. Note that the frequency has been rescaled by J both here and in Fig. 10. At $J/t \lesssim 2.0$ the dispersion has a smooth maximum at $q=\pi$ and seems to approach zero linearly as $q \to 0$. As J/t increases toward the transition point, the peak positions in $S_{zz}(q,\omega)_{t\text{-}J}$ gradually shift to lower values of ω/J, most rapidly at q near π.

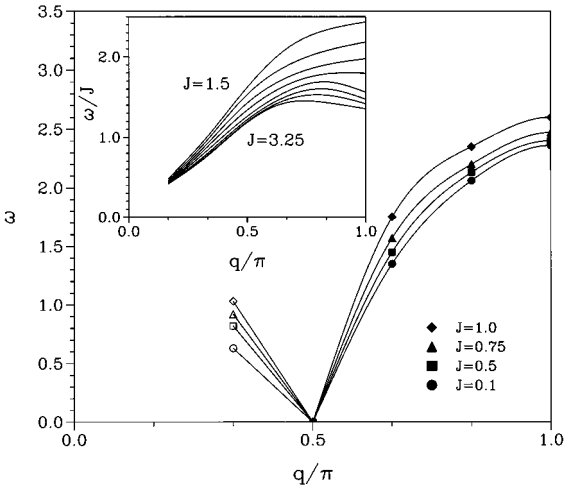

FIG. 8. Dynamically relevant dispersions of the excitations dominating the dynamic spin structure factor $S_{zz}(q,\omega)$ at $T=0$ for $t=1$ and different values of J in the first regime (main plot) and the second regime (inset) of the Luttinger-liquid phase of the t-J model. The symbols, which are smoothly interpolated by solid lines, represent the peak position of results such as shown in Figs. 7 and 10.

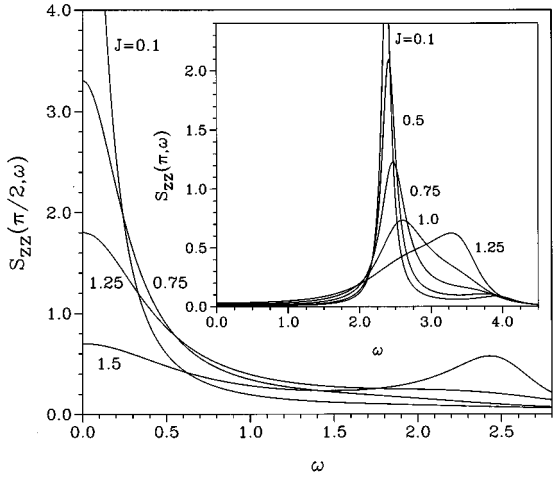

FIG. 9. Line shape at $q=\pi$ (inset) and $q=\pi/2$ (main plot) of the dynamic spin structure factor $S_{zz}(q,\omega)$ at $T=0$ for $t=1$ and various values of J in the first regime of the Luttinger-liquid phase of the t-J model. The results are obtained by the same method as those in Fig. 5.

IV. PHASE SEPARATION

The transition from the Luttinger-liquid phase to a phase-separated state in $H_{t\text{-}J_z}$ takes place at $J_z/t=4$. The equivalent XXZ model undergoes a discontinuous transition to a state with ferromagnetic long-range order at the corresponding parameter value $(J_\parallel/J_\perp=1)$. The ground state at the transition is noncritical and degenerate even for finite N. The XXZ order parameter, $M=N^{-1}\Sigma_l S_l^z$, commutes with H_{XXZ}.

Notwithstanding the exact mapping, the transition of $H_{t\text{-}J_z}$ at $J_z/t=4$ is of a different kind. Only one of the $N+1$ vectors which make up the degenerate XXZ ground state at $J_\parallel/J_\perp=1$ is contained in the invariant subspace that also includes the t-J_z ground state. The other vectors correspond to t-J_z states with different numbers N_e of electrons. The t-J_z ground state at $J_z/t=4$ for fixed $N_e=N/2$ is nondegenerate and represented by the wave function $|\phi_0\rangle$ as given in Eq. (3.3).

The fully phase-separated state as represented by the wave function

$$|\phi_1\rangle \equiv \frac{1}{\sqrt{2N}} \sum_{l_1=1}^{N} |l_1, l_1+1, \ldots, l_1+N/2-1\rangle \times \{|\uparrow\downarrow\uparrow\cdots\rangle \pm |\downarrow\uparrow\downarrow\cdots\rangle\} \tag{4.1}$$

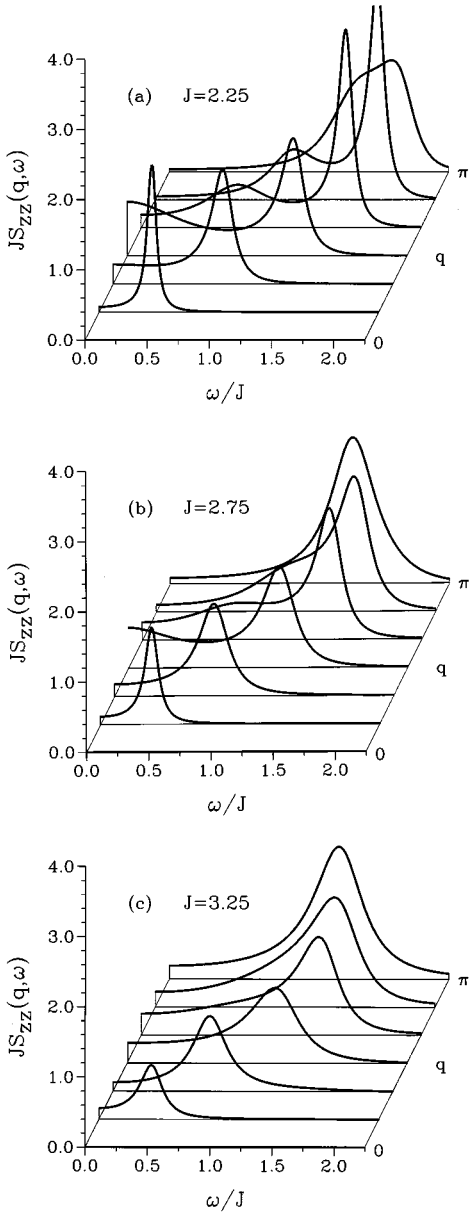

FIG. 10. Dynamic spin structure factor $S_{zz}(q,\omega)$ at $T=0$ in the second regime of the Luttinger-liquid phase of the t-J model. The results for $t=1$ and three different values of J are obtained by the same method as those in Fig. 5.

has an energy expectation value at $J_z/t=4$, $\langle E_1\rangle=-t(N-2)$, which exceeds the finite-N ground-state energy, $E_0=-tN$, pertaining to $|\phi_0\rangle$. However, by comparing the J_z dependence of the energy expectation values (per site) of the two wave functions $|\phi_0\rangle$ and $|\phi_1\rangle$,

$$\tilde{e}_0 \equiv \frac{1}{N}\langle\phi_0|H_{t\text{-}J_z}|\phi_0\rangle = -t-\frac{1}{2}\left(\frac{J_z}{4}-t\right)\left(1-\frac{1}{N-1}\right),$$

$$\tilde{e}_1 \equiv \frac{1}{N}\langle\phi_1|H_{t\text{-}J_z}|\phi_1\rangle = -\frac{J_z}{4}\left(1-\frac{2}{N}\right),$$

in the vicinity of the transition, $J_z/t=4(1+\epsilon)$, we obtain

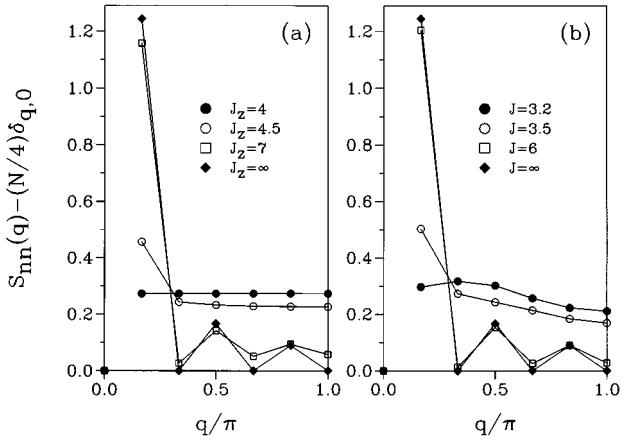

FIG. 11. Static charge structure factor at $T=0$ of (a) the t-J_z model and (b) the t-J model in the phase-separated state. Results extracted from the ground-state wave function determined numerically for systems of $N=12$ sites.

$$\tilde{e}_0-\tilde{e}_1 \xrightarrow{N\to\infty} \frac{\epsilon}{2t},$$

which implies that a level crossing between $|\phi_0\rangle$ and $|\phi_1\rangle$ occurs at $J_z/t=4$ in the infinite system. Moreover, from exact Bethe-ansatz calculations for the XXZ model,[41] we know that the t-J_z ground-state energy per site at $J_z/t>4$ is equal to $\tilde{e}_1$ in the limit $N\to\infty$. This proves that a first-order transition takes place in the infinte t-J_z chain at $J_z/t=4$ between a state with no charge correlations at all and the fully phase-separated state.

The transition to phase separation in $H_{t\text{-}J_z}$ is characterized by the charge and spin order parameters

$$Q_\rho=\frac{1}{N}\sum_{l=1}^{N} e^{i2\pi l/N}n_l, \quad Q_\sigma=\frac{1}{N}\sum_{l=1}^{N} e^{i\pi l}S_l^z.$$

Neither operator commutes with $H_{t\text{-}J_z}$. The phase-separated state of $H_{t\text{-}J_z}$ is characterized, for $N\to\infty$, by a broken translational symmetry, $\langle Q_\rho\rangle\neq 0$, and a broken spin-flip symmetry, $\langle Q_\sigma\rangle\neq 0$.

In the t-J model, the transition to the phase-separated state, which takes place at $J/t\simeq 3.2$, produces charge long-range order, $\langle Q_\rho\rangle\neq 0$, but is not accompanied by the onset of spin long-range order, $\langle Q_\sigma\rangle=0$. The similarities in the charge correlations and the differences in the spin correlations of the two models are evident in the finite-size static charge and spin structure factors.

A. Charge structure factor

The vanishing charge correlations in the finite-size t-J_z ground state at the onset of phase separation ($J_z/t=4$) is reflected in the flat charge structure factor $S_{nn}(q)$ as shown in Fig. 11(a). The corresponding t-J result for $J/t\simeq 3.2$ as shown in Fig. 11(b) indicates that correlated charge fluctuations do exist at the transition.

With the exchange coupling increasing beyond the transition point, the charge structure factors of the two models become more and more alike and reflect the characteristic

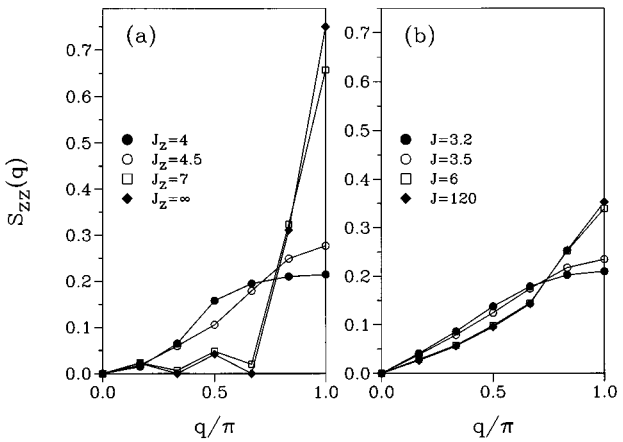

FIG. 12. Static spin structure factor at $T=0$ of (a) the t-J_z model and (b) the t-J model in the phase-separated state. Results extracted from the ground-state wave function determined numerically for systems of $N=12$ sites.

signature of phase separation. Phase separation is associated with an enhancement of $S_{nn}(q)$ in the long-wavelength limit. Because of charge conservation, this enhancement is manifest, in a finite system, not at $q=0$ but at $q=2\pi/N$. It is conspicuously present in the data for couplings $J_z/t=4.5$ and $J/t=3.5$, not far beyond the transition point.

The charge correlation function for the fully phase separated state, as represented by the wave function (4.1), is a triangular function,[42] $\langle n_l n_{l+m}\rangle = 1/2 - |m|/N$, $|m| \leq N/2$. This translates into a charge structure factor of the form

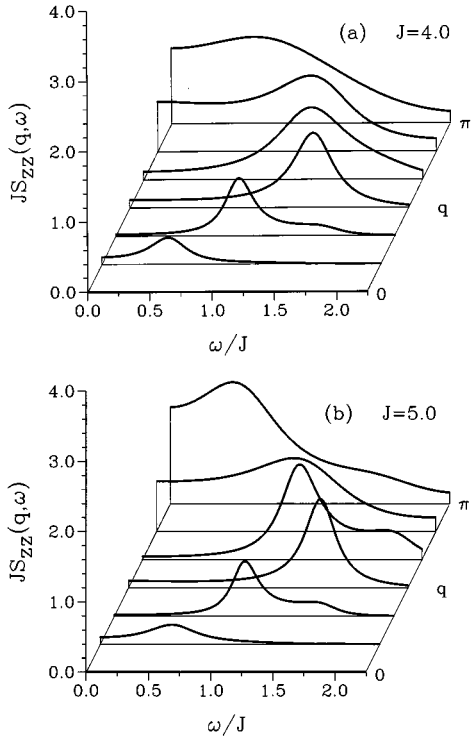

FIG. 13. Dynamic spin structure factor $S_{zz}(q,\omega)$ at $T=0$ in the phase-separated state of the t-J model. The results for $t=1$ and two values of J are obtained by the same method as those in Fig. 5.

$$S_{nn}(q) = \frac{N}{4}\delta_{q,0} + \frac{1+\cos(Nq/2)}{N(1-\cos q)}(1-\delta_{q,0}), \qquad (4.2)$$

as shown (for $N=12$) by the full diamonds in Fig. 11. This function vanishes for all wave numbers $q=2\pi l/N$ with even l and increases monotonically with decreasing odd l. The data in Fig. 11 suggest that the phase separation is nearly complete before the exchange coupling has reached twice the value at the transition. In the t-J_z case, we already know that complete phase separation is established (for $N\to\infty$) right at the transition.

B. Spin structure factor

The extremely short-ranged spin correlations in the t-J_z ground state (3.3) for $N\to\infty$ are reflected by the static spin structure factor (3.7). For finite N the spin correlations at distances $|n|\geq 2$ do not vanish identically. An exponential decay is observed instead with a correlation length that dis-

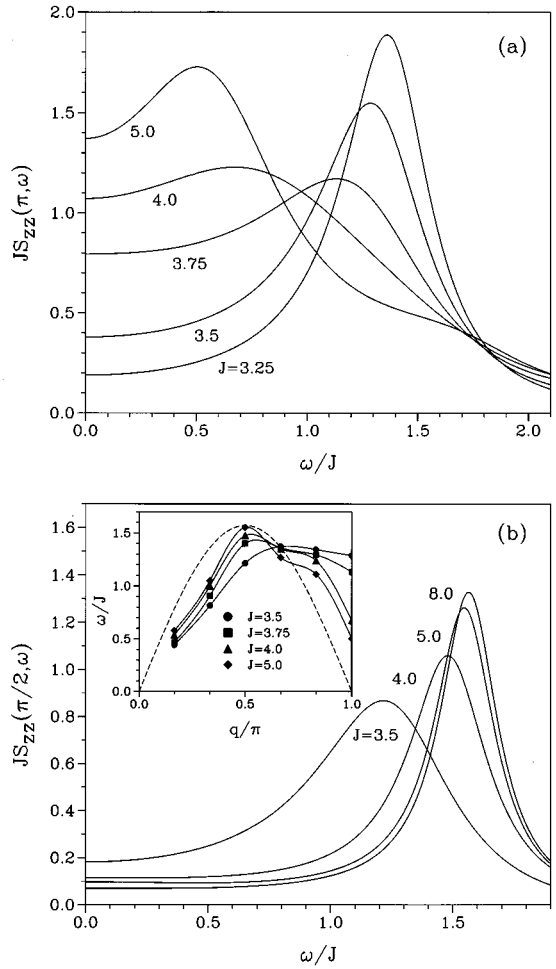

FIG. 14. Line shape of the dynamic spin structure factor (a) $S_{zz}(\pi,\omega)$ and (b) $S_{zz}(\pi/2,\omega)$ of the t-J model in the phase-separated state. The results for $t=1$ and various values of J are obtained by the same method as those in Fig. 5. Inset: Dynamically relevant dispersions of the excitations dominating the dynamic spin structure factor $S_{zz}(q,\omega)$ at $T=0$ for $t=1$ and different values of J in the phase-separated state of the t-J model. The symbols which are smoothly interpolated by solid lines represent the peak position of results such as shown in Fig. 13.

appears as $N\to\infty$. Hence the difference between Eq. (3.7) and the finite-N data depicted in Fig. 12(a) (●). The t-J spin structure factor near the transition ($J/t\simeq 3.2$) has a similar q dependence except at small q, where it tends to zero linearly instead of quadratically.

Whereas the charge structure factors of the two models become more and more alike as the exchange coupling increases in the phase-separated state (Fig. 11), divergent trends are observed in the respective spin structure factors, on account of the fact that the t-J_z model supports spin long-range order, and the t-J model does not.

The fully phase-separated state of the t-J_z model is at the same time fully Néel ordered. The spin correlation function in the state (4.1) reads $\langle S_l^z S_{l+m}^z\rangle=(1/4)(-1)^m(1/2-|m|/N), |m|\leqslant N/2$, and the corresponding spin structure factor has the form

$$S_{zz}(q)=\frac{N}{16}\delta_{q,\pi}+\frac{1-\cos[N(\pi-q)/2]}{4N[1-\cos(\pi-q)]}(1-\delta_{q,\pi}). \quad (4.3)$$

The function (4.3) vanishes (for even $N/2$) at all wave numbers $q=2\pi l/N$ with even l, just as Eq. (4.2) did. The exception is the wave number $q=\pi$, where $S_{zz}(q)$ assumes its largest value.

The t-J spin structure factor evolves quite differently in the presence of increasing phase separation as is illustrated in Fig. 12(b). The electron clustering produces in this case the Heisenberg antiferromagnet, whose ground state is known to stay critical with respect to spin fluctuations. The spin structure factor of that model is known to be a monotonically increasing function of q, which grows linearly from zero at small q and (for $N\to\infty$) diverges logarithmically at $q=\pi$.[18]

C. Spin dynamics (t-J model)

The charge long-range order in the phase-separated state freezes out the charge fluctuations in both models, and the accompanying spin long-range order in the t-J_z model freezes out the spin fluctuations too. What remains strong are the spin fluctuations in the t-J model.

At the transition to phase separation ($J/t\simeq 3.2$), the $q=\pi$ spin mode in $S_{zz}(q,\omega)_{t\text{-}J}$ does not go soft. However, the gradual electron clustering tendency in conjunction with the continued strengthening of the antiferromagnetic exchange interaction brings about a softening in frequency and an enhancement in intensity of the order-parameter fluctuations associated with Néel order. Both effects can be observed in the reconstructed dynamic spin structure factors at $J/t=3.25$, 4.0, 5.0 as shown in Figs. 11(c), 13(a), and 13(b).

A close-up view of the gradual transformation of the $q=\pi$ mode is shown in Fig. 14(a). For sufficiently strong exchange coupling, the function $S_{zz}(\pi,\omega)_{t\text{-}J}$ will be characterized by a strong, i.e., nonintegrable infrared divergence, $\sim\sqrt{-\ln\omega}/\omega$,[43] which characterizes the order-parameter fluctuations of the 1D $s=1/2$ XXX antiferromagnet.

Figure 14(b) shows the gradual change in line shape and shift in peak position of the function $S_{zz}(\pi/2,\omega)_{t\text{-}J}$ in the phase-separated state. The peak, which starts out relatively broad at the transition, shrinks in width, loses somewhat in intensity, and moves to a higher frequency. For $J/t\gtrsim 5.0$ it settles at $\omega/J\simeq\pi/2$ in agreement with the lower boundary, $\omega_L(q)=(\pi J/2)|\sin q|$, at $q=\pi/2$ of the two-spinon continuum. The width has shrunk to a value consistent with the width of the two-spinon continuum at that wave number.

In the inset to Fig. 14 we show the evolution of the dynamically relevant dispersion for $S_{zz}(q,\omega)_{t\text{-}J}$ in the phase-separated state, as determined by the peak positions of our data obtained via SCCF reconstruction. The dashed line represents the exact lower threshold of the two-spinon continuum. The shift of the peak positions in our data is directed toward that asymptotic position at all wave numbers for sufficiently large J/t.

ACKNOWLEDGMENTS

This work was supported by the U. S. National Science Foundation, Grant No. DMR-93-12252, and the Max-Kade Foundation. Computations were carried out on supercomputers at the National Center for Supercomputing Applications, University of Illinois at Urbana-Champaign.

*Present address: C.W. Costello & Associates, Providence, RI 02903.

[1] F. C. Zhang and T. M. Rice, Phys. Rev. B **37**, 3759 (1988); C. Gros, R. Joynt, and T.M. Rice, *ibid*. **36**, 381 (1987).
[2] C. S. Hellberg and E. J. Mele, Phys. Rev. Lett. **67**, 2080 (1991).
[3] F. F. Assaad and D. Würtz, Phys. Rev. B **44**, 2681 (1991).
[4] T. Pruschke and H. Shiba, Phys. Rev. B **44**, 205 (1991).
[5] M. Ogata, M. U. Luchini, S. Sorella, and F. F. Assaad, Phys. Rev. Lett. **66**, 2388 (1991).
[6] N. Kawakami and S.-K. Yang, Phys. Rev. Lett. **65**, 2309 (1990); J. Deisz, K.-H. Luk, M. Jarrell, and D. L. Cox, Phys. Rev. B **46**, 3410 (1992); T. Xiang and N. Ambrumenil, *ibid*. **45**, 8150 (1992).
[7] P. Schlottmann, Phys. Rev. B **36**, 5177 (1987); P.-A. Bares, G. Blatter, and M. Ogata, *ibid*. **44**, 130 (1991).
[8] T. Tohyama, P. Horsch, and S. Maekawa, Phys. Rev. Lett. **74**, 980 (1995).
[9] H. Yokoyama and M. Ogata, Phys. Rev. Lett. **67**, 3610 (1991); Phys. Rev. B **53**, 5758 (1996).
[10] E. Lieb, T. Schultz, and D. Mattis, Ann. Phys. (N.Y.) **16**, 407 (1961).
[11] S. Katsura, Phys. Rev. **162**, 1508 (1962).
[12] T. Niemeijer, Physica **36**, 377 (1967); S. Katsura, T. Horiguchi, and M. Suzuki, *ibid*. **46**, 67 (1970).
[13] A. Parola and S. Sorella, Phys. Rev. Lett. **64**, 1831 (1990).
[14] M. Ogata and H. Shiba, Phys. Rev. B **41**, 2326 (1990).
[15] The first part of Eq. (2.10) was previously given in Ref. 13. The techniques used to perform this kind of asymptotic expansion were explained by T. Tonegawa, Solid State Commun. **40**, 983 (1981).
[16] B. M. McCoy, Phys. Rev. **173**, 531 (1968).
[17] B. M. McCoy, J. H. H. Perk, and R. E. Shrock, Nucl. Phys. **220** [FS8], 35 (1983); **220** [FS8], 269 (1983).
[18] R.R.P. Singh, M.E. Fisher, and R. Shankar, Phys. Rev. B **39**, 2562 (1989); I. Affleck, D. Gepner, H.J. Schulz, and T. Ziman, J. Phys. A **22**, 511 (1989).
[19] We have fitted the asymptotic term to the data for $N_e=4,6,\ldots,28$ and extrapolated the sequence of amplitudes.

[20] What this simple argument does not explain is why the spin correlations are stronger ($\sim m^{-1/2}$ or $m^{-3/2}$) than the charge correlations (m^{-2}).
[21] J. Stolze, V.S. Viswanath, and G. Müller, Z. Phys. B **89**, 45 (1992).
[22] J. Stolze, A. Nöppert, and G. Müller, Phys. Rev. B **52**, 4319 (1995).
[23] References on the properties of Pfaffians and their use for the calculation of many-fermion correlations can be found, for example, in the Appendix of Ref. 21.
[24] We have set the energy unit of Eq. (1.1) equal to unity ($t=1$) here, in order to avoid confusion with the time variable.
[25] H. G. Vaidya and C. A. Tracy, Physica **92A**, 1 (1978); G. Müller and R. E. Shrock, Phys. Rev. B **29**, 288 (1984).
[26] R. Haydock, in *Solid State Physics: Advances in Research and Applications*, edited by H. Ehrenreich, F. Seitz, and D. Turnbull (Academic, New York, 1980), Vol. 35, p. 215; M. H. Lee, Phys. Rev. B **26**, 2547 (1982); E. R. Gagliano and C. A. Balseiro, *ibid*. **38**, 11 766 (1988).
[27] V. S. Viswanath and G. Müller, *Recursion Method - Application to Many-Body Dynamics*, Lecture Notes in Physics, Vol. 23 (Springer-Verlag, New York, 1994).
[28] V. S. Viswanath, S. Zhang, J. Stolze, and G. Müller, Phys. Rev. B **49**, 9702 (1994).
[29] V. S. Viswanath, S. Zhang, G. Müller, and J. Stolze, Phys. Rev. B **51**, 368 (1995).
[30] A. Fledderjohann, M. Karbach, K.-H. Mütter, and P. Wielath, J. Phys. Condens. Matter **7**, 8993 (1995).
[31] C. N. Yang and C. P. Yang, Phys. Rev. **150**, 321 (1966); **151**, 258 (1966).
[32] J. Des Cloizeaux and M. Gaudin, J. Math. Phys. **7**, 1384 (1966).
[33] A. Luther and I. Peschel, Phys. Rev. B **12**, 3908 (1975); F.D.M. Haldane, Phys. Rev. Lett. **45**, 1358 (1980).
[34] T. Schneider, E. Stoll, and U. Glaus, Phys. Rev. B **26**, 1321 (1982).
[35] H. Beck and G. Müller, Solid State Commun. **43**, 399 (1982).
[36] This cusp was also observed at $J/t \gtrsim 1$ in the Monte Carlo data of Ref. 3 for considerably larger systems.
[37] See Figs. 4(b) and 9 in Ref. 29 for the t-J_z and t-J results, respectively.
[38] J.D. Johnson, S. Krinsky, and B. M. McCoy, Phys. Rev. A **6**, 1613 (1973).
[39] The continued-fraction coefficients in Eq. (3.1) are found to have the symmetry property $\Delta_k^z(q)=\Delta_k^z(\pi-q)$, whereas the integrated intensity $S_{zz}(q)$ remains asymmetric.
[40] A quantitative analysis of t-J spin dispersions at $0 \leqslant q \leqslant \pi/2$ in this coupling range requires data for longer chains.
[41] G. Albertini, V.E. Korepin, and A. Schadschneider, J. Phys. A **28**, L303 (1995).
[42] See, e.g., Fig. 8(f) of Ref. 3.
[43] A.H. Bougourzi, M. Couture, and M. Kacir, Phys. Rev. B **54**, R12 669 (1996); M. Karbach, G. Müller, A.H. Bougourzi, A. Fledderjohann, and K.-H. Mütter, *ibid.* (to be published).